JMEPEG (2012) 21:2131–2139
DOI: 10.1007/s11665-012-0154-y

1059-9495/$19.00

Study on the Microstructures and Tensile Behaviors of Friction Stir Welded T-joints for AA6061-T4 Alloys

G. Zhou, X.Q. Yang, L. Cui, Z.H. Zhang, and X.D. Xu

(Submitted July 16, 2011; in revised form December 13, 2011)

Friction stir welding (FSW) of T-joints with 3 mm thickness for AA6061-T4 sheets has been performed, and the influences of process parameters on the microstructures, defects, hardness profiles, and tensile strength were discussed specifically. It is found that the macrostructures and microstructures are similar in different process parameters, and the microstructure features in the skin welds have the same patterns as that of butt-joints. The unique microstructures of T-joints are the two fillet zones. Two lower hardness zones in the skin and one lower hardness zone in the stringer are found. Additionally, the tensile properties of T-welded joints are examined along the skin and the stringer plane directions. Results show that the tensile strength is in the range of 170-180 MPa for all the specimens along the skin direction, and the specimens fail in the heat affected zone (HAZ). In the stringer direction, the larger tunnel defects (DA) (the DA is greater than 0.1 mm^2) would reduce the ultimate tensile strength of the T-joints and cause the joints to fracture at the bonding interface. The smaller tunnel defects (the DA is less than 0.015 mm^2) and the zigzag lines have no pronounced effect on the failed location. In the stringer direction, tensile efficiencies of T-joints could be 83% of the base material (BM) when ω/v = 1541/218 r/mm is applied.

Keywords aluminum, mechanical Testing, welding

1. Introduction

As a relatively novel solid-state joining technique, friction stir welding (FSW) has been considered to be one of the most significant developments in metal joining fields in the two decades. The basic process of FSW is that the non-consumable rotating tool with a probe and shoulder is inserted into the abutting edges of two plates and moved along the joining line. During the process of FSW, material undergoes intense plastic deformation at elevated temperature, resulting in the better modification of microstructures and mechanical properties (Ref 1).

Now, it is confirmed that FSW has the greatly potential applications in the transport and automobile fields, especially for the airplane and aerospace industries due to relevant advantages. Currently, most work is being performed for the butt configurations of either similar or dissimilar aluminum, magnesium or steel sheets. FSW process has been successfully introduced into several applications, such as the jet aircraft Eclipse 500, the propellant tanks for the Boeing Delta IV launch vehicle and the Japanese Shinkansen (Ref 2, 3). However, there are only a few of results on overlap joints or the other configurations (Ref 4). The lack of information about the other complex joints (such as T-welded joints, corner welded joints, and box sections) will restrict the further widespread applications of FSW technology.

G. Zhou, X.Q. Yang, L. Cui, Z.H. Zhang, and **X.D. Xu**, Tianjin Key Laboratory of Advanced Joining Technology, School of Materials Science and Engineering, Tianjin University, Tianjin, China. Contact e-mail: xqyang@tju.edu.cn.

T-joints are one of the important joining shapes for industrial applications. One of the important features of T components is that the stiffness and strength of skins (the horizontal sheets) can be remarkably reinforced by stringers (the vertical sheets) without a significant increase in weight (Ref 2) It is well known that the 'skins and stingers' joints are always used for flying structure bodies, T-lap welded joints are often utilized in the car back supports seats, and hermetically closed boxes are used for the cooling elements and heat exchangers (Ref 5, 6). T-joints can be obtained by extrusion processes for aluminum alloys, but the overall manufacturing costs are always higher and the sizes of components are also limited. Therefore, it is very necessary to perform the deep investigation on T-joints by FSW. Recently, more and more investigators have paid attentions to FSW of T-joints. And several positive results have been published for the T-joints of aluminum alloys, focusing on the material flow, the optimization of welding technologies, the microstructure features, and mechanical properties.

It is essential to obtain the patterns and features of material flow during FSW process to understand the joining mechanism and the formation of defects. Some of the efforts have been done for the material flow of T-joints based on the numerical simulations of finite element method (FEM) and the experiments of marker techniques. Buffa et al. (Ref 5) studied the material flow of T-joints for AA2024-T4 by using experimental observation. They found that during T-welding the material flowed to the downward and outward to form the fillets, and in the skin of T-joint the flow pattern was similar to that in the FSW butt joint. The FEM simulations of the material flow of T-joints were also performed and verified to be consistent with the experimental observations (Ref 5, 7).

The welding parameters (the plunge depth or forging force, the rotational and moving speed) and the tool parameters (the shoulder diameter, the probe shapes, and dimensions) should be the key factors to influence the mechanical properties of

T-joints during FSW (Ref 8). In the past two decades, many investigations have been conducted on the parameter optimization of butt-joints. But most of the parameters obtained from butt-welding are not suitable for T-joints. This is because that the material flow patterns and the joining conditions of the two types of joints are really different. In butt-joints, the surfaces to be welded are parallel to the probe axis of the tool, while the joining interfaces are horizontal or vertical and horizontal in T-joints. The optimization of FSW of T-joints indicated that the tool characterized by large shoulder diameters were helpful to produce sufficient material flow and obtain sound joints (Ref 8). Additionally, the tool with cylindrical probe would cause the formation of some flow defects, while the tool with conical probe would cause the formation of sharper surfaces (Ref 7).

In order to keep the precise shape and position between the skin and the stringer, T-joints are performed on a special clamping fixture. The designed fixtures in published investigations were characterized by two fillet radii for each side of the joint and by the significant gaps near the weld zone (Ref 9, 10). Material flow must be sufficient to fill the radius sites of fixture through the forging action of the tool. The fillets with larger radii require the more material to be extruded to form the fillet sites, making the top skin thinner. The fillets with smaller radii need the less material to fill the fillets, producing the risk for the FSW tool to contact and destroying the backing plate surface. Erbsloh (Ref 11) reported that the rounded fillet radii that were influenced by the backing plate also increased the propensity of crack formation. So, the fit situation between the probe shapes and fillets should be important additional considerations to protect the tool and to produce sound T-welds.

The mechanical properties of T-joints are also performed by several groups. Tensile tests are carried out by pulling the skin or the stringer, respectively. Fratini et al. (Ref 8) used T-pull fixture to estimate the tensile properties of T-welds. They found that, when AA2024-T4 and AA7075-T6 alloys T-joints were welded, tensile efficiencies of T-joints was 67-87% of the base material (BM) (AA2024-T4). Tavares et al. (Ref 12) made a comparison of the tensile performances of T-joints transversally to the weld line with BM and butt-joints for the AA 6056-T4 alloys. Results showed that weld efficiencies, 73% of BM, could be obtained for T-joints in tensile testing but with the drawback of the loss of elongation. Furthermore, the other researchers performed some investigations on the mechanical properties of FSW T-joints undergoing bending, and such results were compared with that of the fusion welded T-joints (Ref 13).

What is more, the understanding of microstructural evolution in FSW T-welds is really important to acquire the optimal mechanical properties of welded joints. Several experiments were performed to explore the evolution of microstructures in T-welds. Fine grains and specific microstructures with the multiple nuggets could be observed in the T-welds. And the transition between nugget and the thermo-mechanically affected zone (TMAZ) was the weaker point of the junction (Ref 2, 14).

However, it should be emphasized that the published researches on FSW T-joints are really deficient. In the present study, the friction stir welded T-joints of two sheets with the same thickness (3 mm) were performed, and the influences of process parameters on the microstructures, corner defects, hardness profiles, and tensile properties were discussed specifically. The widely used AA6061-T4 was selected as the experiment material. The initial welding parameters were referred to the published experimental results (Ref 7, 13, 14). The further modified parameters were determined based on the macro-observation of the T-welds of testing specimens. After welding, the metallographic examinations and tensile testing were performed to evaluate the welding qualities and mechanical properties of the FSW T-joints.

2. Experimental

The rolled plates of 3 mm thickness, AA6061-T4 (solution heat-treated and naturally aged) aluminum alloy, were welded by FSW. The chemical composition of AA6061-T4 is shown in Table 1. The skins and stringers were machined into the rectangular testing plates of 300 × 95 mm and 300 × 65 mm, respectively. The weld tool made of the H13 steel was tempered up to 52 HRC, and the shoulder surface was the concave shape.

Before welding, the welded surfaces of skins were prepared to remove the oxide. The initial T-configurations of joints were obtained by using the special fixtures. The shape and structure of fixed T-joint is shown in Fig. 1.

During welding process, the axis of tool probe titled 2.5° from the normal direction of the welded-plate was employed. Rotation speeds (ω) of 1008, 1541, and 2256 rpm, and welding speeds (v) of 75, 142, and 218 mm/min were used. The probe of rotating tool completely pierced through the thickness of skin and partially penetrated into the edges of stringer. The shoulder of the rotating tool was closely pressured on the upper surface of the skin. Meanwhile, the tool was moved along the jointed line to form the T-welds. Nine T-joints were produced by the combination of process parameters.

For metallographic examination, the specimens perpendicular to the FSW direction were cut along the across section of T-welds. The specimen sizes should be large enough to contain the whole different zones of T-welds. Then the specimens were milled, polished, and etched by the Keller's reagent (the composition is 1% HF, 1.5% HNO_3, 2.5% HCl in volume). Microstructural investigation was conducted using the optical microscopy on the cross-sections of the welds. Then the microhardness profiles corresponding to the local microstructures were tested specifically.

Table 1 Chemical compositions (all compositions are in wt.%) of the base materials

Material	Si	Fe	Cu	Mn	Mg	Zn	Ti	Al
6061	0.1-0.8	0.7	0.15-0.40	0.15	0.8-1.2	0.25	0.15	Balance

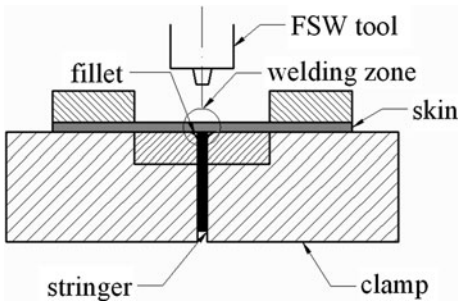

Fig. 1 The shape and structure of FSW T-welded joint

The tensile tests were carried out at room temperature to evaluate the mechanical properties of T-joints obtained in the different welding conditions. Before tensile testing, all the specimens were placed in the laboratory for 3 months after welding to ensure that the stable states of natural aging welds could be reached. All specimens with macro-defect-free by the visual inspection of the weld corners and crowns were produced by employing the electrical discharge processing. The tensile specimens with 25 mm width were tested on a servo-hydraulic machine by displacement control mode at the speed of 1 mm/min. Three tensile specimens were carried out for each welding condition. The loading directions were applied along the stringer/longitudinal (L) and skin/transversal (T) plane directions, respectively (Fig. 2). The longitudinal tensile testing was performed by using special clamps that could fix the skin with nearly zero flexural torque situations. In this way, the stringers were vertically pulled from the T-weld of skin at last.

3. Results and Discussion

3.1 Macrostructure and Microstructure

It can be seen from Fig. 3(a) that there is nearly no distortion for FSW T-joints, compared with that of fusion welding methods. Smooth fillets as shown in Fig. 3(b) are observed in all of the T-joints. The top surface of T-welds is characterized by some stir features (semicircular striping marks) as a consequence of shoulder rotation and by an exit hole (Fig. 3c). However, a little amount of flash is formed at the top surface due to surface overheating at high rotation speed (2256 rpm). At the low rotation speed (1008 rpm), the incomplete bonding exists at the fillet with relatively smooth top surface. The perfect joints are produced at the rotation speed of 1541 rpm.

The typical macrostructures of the cross-section of T-joints are presented in Fig. 4. The macrostructural observations of cross-section indicates that the specimens do not show the features of representative FSW onion rings because of the non-threaded probe and high rotation speeds. Nugget zone (NZ) is larger than the probe diameter and extends into the stringer. The shape of NZ is an inverted trapezoid with two curved edges (the interfaces between the NZ and TMAZ) which are highlighted by blue lines in Fig. 4(a). It is probably caused by a

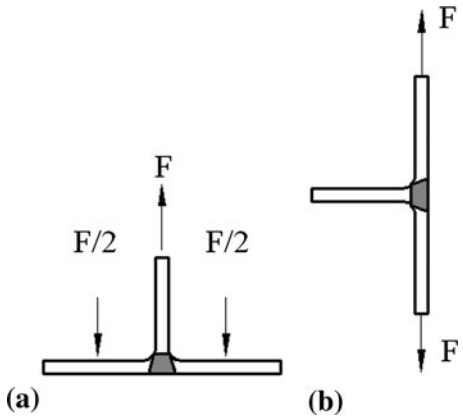

Fig. 2 Tensile loading mode of T-welds (a) along stringer plane (L), (b) along skin plane (T)

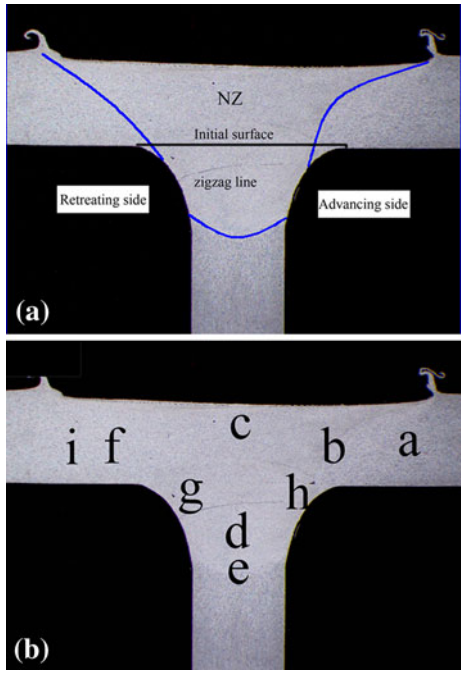

Fig. 4 The macrostructures of the transverse section of T-joints (a) ω/v = 1541/142 r/mm, (b) ω/v = 2256/142 r/mm

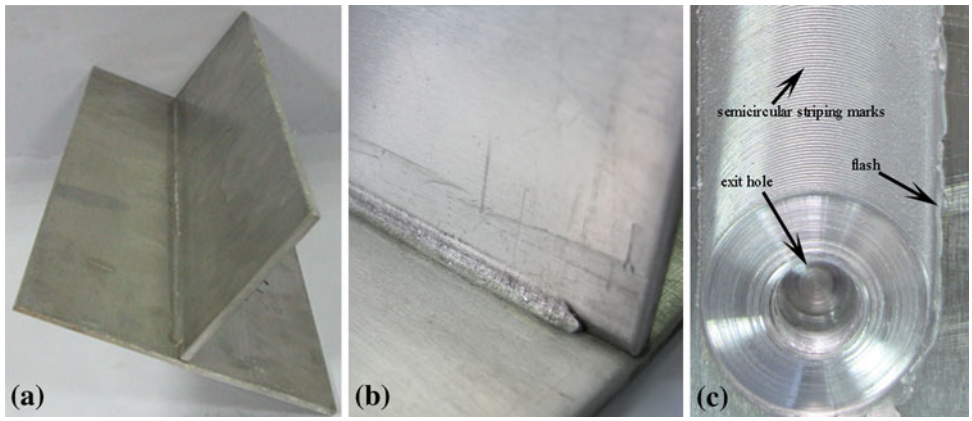

Fig. 3 The macro-photographs of T-joints (a) the whole view of T-joint, (b) the fillet, (c) the top surface

combination of conical probe, rigid fixture, and material flow. The conical probe stirs the material to form the top half zone of trapezoid as the butt-joints. The rest zone of the trapezoid is made up from the two fillets of the fixture and a part of the stringer. And this zone restricts the material flow and forms the lower part of nugget during FSW process. It was found in the previous studies that two classified shapes of nuggets (basin-shaped and elliptical nuggets) could be observed in butt-joints and lap-joints (Ref 1, 15). Although the basin-shaped nuggets for butt-joints and lap-joints are similar to the inverted trapezoid nuggets for T-joints, the formation mechanism of NZ for the former is a little different from that of the latter. The formation of the lower part of inverted trapezoid nuggets with two curved edges in the FSW T-joint is mainly due to the constraint of rigid fixtures, but the rigid fixing is lack in the butt-joints or lap-joints.

Another typical feature in the T-welds is the dark 'zigzag' line in the neighbors of bonding interfaces (Fig. 4a). Zigzag line would be considered to be composed of oxide particles existed at the initial surfaces of BM. Oxide particles are entrapped into T-welds during welding. In our experiment, we find that these dark wavy lines, which are nearly perpendicular to the tool axis and are similar to the position of faying surface in lap-joints (Ref 16), occur from the AS to RS at the down NZ. However, the zigzag lines in FSW butt-joints are always observed at the root sites of friction stir welds or in the whole welds due to the insufficient stirring actions of tool probe (Ref 17, 18).

Although the zigzag lines are regarded as one types of special defects existed in FSW, they also could be considered as the nature markers to describe the material flow of T-joints. In the advancing side (AS), the lines are obscure and straight. In turn, they become clear and curved in the retreating side (RS). Therefore, it can be concluded that the material flow moves downward more obviously in the retreating side of T-welds.

It is found that the microstructures of all the specimens are similar in different welding conditions. Table 2 gives a summary of the approximate grain size values in different FSW conditions. The process parameter of ω/v = 2256/142 r/mm is selected as one of the typical examples to perform detailed metallographic examination. In Fig. 4(b), all the marked zones are highlighted by Keller's reagent. The sites of (a), (b), (c), (d), (e), (f), (g), (h), and (i) indicate the BM, the transition zone between the TMAZ and the NZ in the AS, the NZ in the skin, the NZ in the stringer, the transition zone between the TMAZ and the NZ in the stringer, the transition zone between the TMAZ and the NZ in the RS, the fillet zone in the RS, the fillet zone in the AS, and the heat affected zone (HAZ), respectively. In order to observe the detailed varying features of T-welded microstructures, the local magnifications of all zones are presented.

Table 2 Process parameters and the grain size values of the nugget zone

Rotating speed (ω), rpm	Welding speed (v), mm/min	ω/v, r/mm	Grain size in the skin, μm	Grain size in the stringer, μm
1008	75	13.44	20	13.3
	142	7.10	18.6	13
	218	4.62	17.3	13
1541	75	20.55	26	16
	142	10.85	25	16
	218	7.07	21.4	15
2256	75	30.08	28	21
	142	15.89	28	21
	218	10.34	25.4	20.5

As shown in Fig. 5(a), the BM contains lots of large secondary phase particles (black particles) that are susceptible to be etched by Keller's reagent. But the boundaries of initial grains are difficult to be etched and be shown by using the optical microscopy.

Figure 5(b) shows the different microstructure features of the NZ and the TMAZ in the AS. The stir actions of tool probe will cause the grains of BM to be drawn into the NZ, and the grains of TMAZ are elongated along the direction of shear stress produced by the speeding rotation of tool probe. No recrystallization phenomena can be observed in these situations of the TMAZ. This is because the temperature caused by the FSW processing is insufficient and the deformation is not so severe to cause recrystallization. However, some large precipitates are dissolved due to the elevated temperature exposure during FSW. The remnant precipitates are dispersed along the material flow line. The shapes of grains in the NZ reveal an obvious reduction in sizes and the density of distribution. From the center of NZ to the interface between NZ and TMAZ, the grains become larger gradually (Fig. 5b and c).The average grain size of NZ is about 40 μm, compared to 150 μm in the TMAZ. The microstructures, near the TMAZ, may be sub-grains resulted from the severe plastic deformation of the material caused by tool shoulder forging and probe stirring actions.

The contribution of severe plastic deformation and higher temperature exposure in the stirred zone results in recrystallization and precipitate dissolution. In butt welds, the average grain size at the bottom side of weld is smaller than that of the top sides (Ref 17). Similarly, the grains in the nugget of the skin are bigger than those in the stringer (Fig. 5c and d). The average grain sizes in the skin and stringer zones are estimated as 28 and 21 μm, respectively. Such a variation in grain size from skin to stringer is associated with the asymmetric heat input and different cooling rate. The highest temperature is produced near the top surface of welds due to top surfaces of skin are fully contacted with the tool shoulder, but the stringers are directly contacted with the backing fixtures and the temperature should be lower than that of skin. Moreover, the heat exchange between the surfaces of welds and atmosphere is slower than that between the stringers and fixtures. So, the relatively higher temperature and the slower heat exchange result in the more quickly growth of grains in the skin. In one word, the comparison of microstructures in the NZ and TMAZ of skin areas with these of butt welds shows similar result.

It should be noted that the morphology of transition zone between the NZ and the TMAZ in the stringer is not apparently different from that of the AS, except the amount of precipitates and grain size values in the NZ (Fig. 5e). However, the formation mechanisms of two transition zones are strikingly different. The bending grains in the stringers are depended on the combination of the friction stir action of probe tip and the friction heat between the probe and the stringer. However, the bending grains in the skin are caused by the shear action of probe profile and the friction heat between the shoulder and the skin.

The transition interfaces between the NZ and the TMAZ in the retreating side are relatively wide and gradually diffused compared to that of advancing side (Fig. 5f). And the result is similar to the FSW butt-joints (Ref 2). This is due to the fact

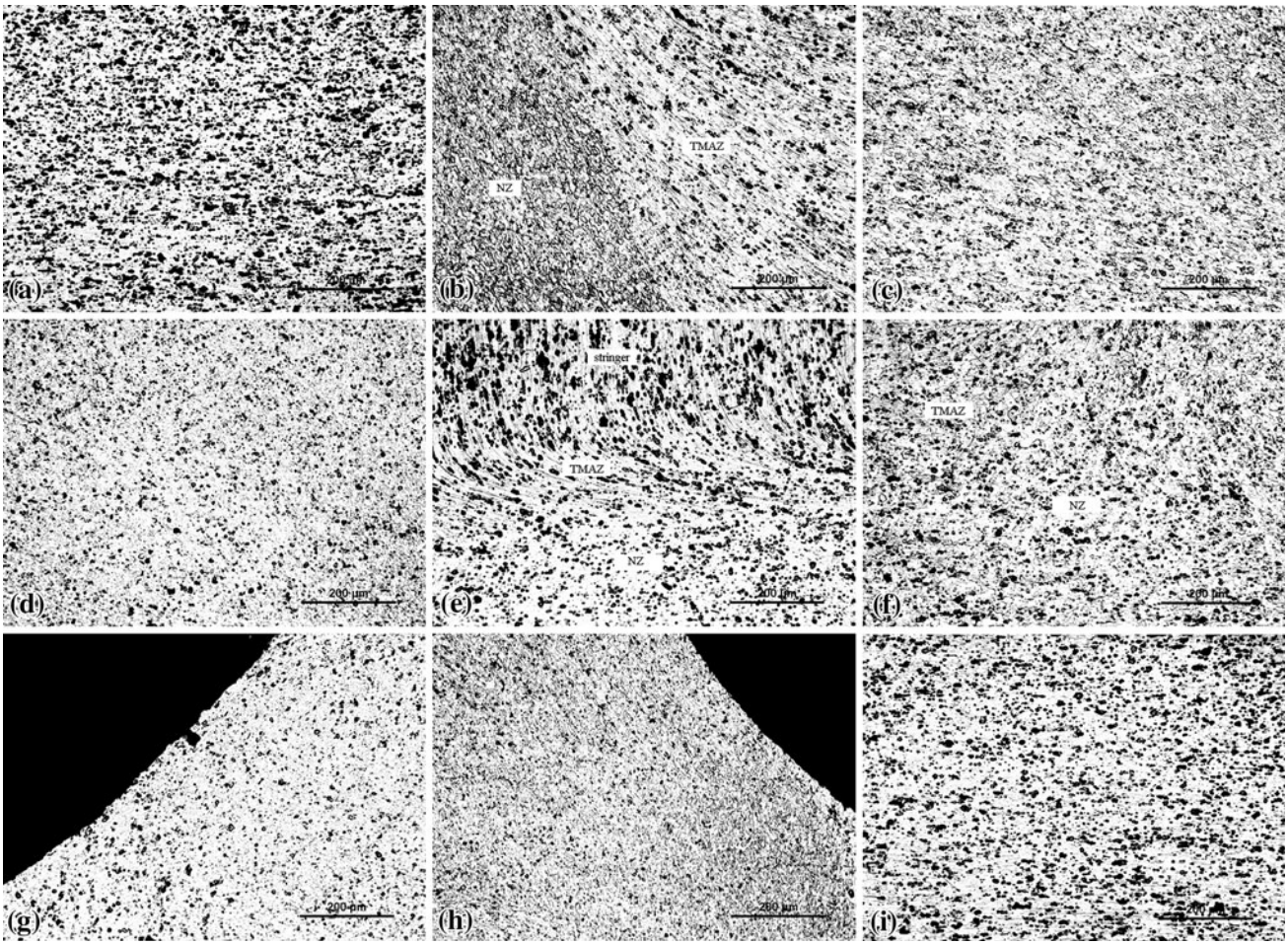

Fig. 5 Microstructures of the T-joints (a) BM, (b) transition zones between TMAZ and NZ in the AS, (c) NZ in the top skin, (d) NZ in the stringer, (e) transition zones between TMAZ and NZ in the stringer, (f) transition zones between TMAZ and NZ in the RS, (g) fillet in the RS, (h) fillet in the AS, (i) HAZ

that the advancing side is characterized by the positive combination of the feed speed and the peripheral tool velocity, but the retreating side has the opposite velocity vectors of feed and rotation (Ref 9).

The unique features of T-joints, as shown in Fig. 5(g) and (h), are the two fillet zones which do not exist in butt- or lap-joints. Fine equiaxed grains in the fillet zone of retreating side are the same as Fig. 5(d). However, the microstructures in the fillet zone of advancing side present multi-morphologies, namely the multi-microstructures including normal grains, fine grains, and bending grains, respectively. Fine grains in the two fillets are attributed to the outward material flow which is caused by the forging and extruding actions of the tool shoulder and the tool probe.

It is found that the grains of HAZ are basically retained the same patterns as those of BMs, since there is no plastic deformation to alter the initial grain structures (Fig. 5i). Parts of the precipitates are vanished during the thermal cycle of the welding process. And the dissolution of the strengthening particles in the matrix may lead to local softening effects.

3.2 Tunnel Defects

FSW joints are free from porosity, hot cracking, and slag inclusion that occur in fusing welding processes. However, for FSW joints, defects such as the tunnels, kiss bonding, and piping defects can be formed. In butt-joints, tunnel defects are found near the bottom of welds in the retreating side due to insufficient material flow refilling towards these zones (Ref 19), or are observed at the triple junction of shoulder flow zone, NZ, and the outside TMAZ at the advancing side (Ref 20). Regarding lap-joints, the faying surfaces (hooking defects) at the advancing side are generally remained outside the nugget and fold upwards along the nugget boundaries, at the retreating side the faying surfaces are lifted up and penetrate into the nugget (Ref 16). In the case of T-joints, there are visible tunnel defects in the fillets of T-joints (Fig. 6). The tunnel defects are tended to appear at the toe corner of stringer nugget along the advancing side in which an abrupt microstructure evolution occurs from the bending grains to fine grains. But the fillet is free from the tunnel defects in the RS.

It is reported that materials flow towards downward and outward to form the fillets of T-welds. In the skin, the material flow behavior is similar to that observed in butt welds (Ref 5). There are two main material flow patterns in the skin zone. First, at the low middle zones of the nugget, materials flow from the AS to the RS. Second, at the upper zones of nugget, materials flow from the RS to the AS (Ref 21). Based the above discussions, one simple model is suggested to explain the formation of tunnel defects for T-joints (Fig. 7). When the

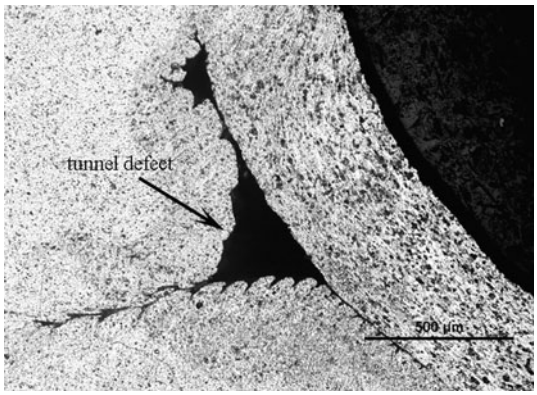

Fig. 6 Tunnel defect of T-joint at the toe corner of stringer nugget along advancing side when ω/v = 1008/75

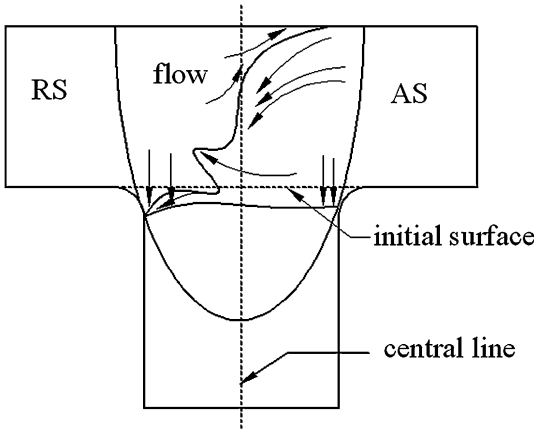

Fig. 7 Material flow model in T-joints

welding parameters are suitable for FSW processes, the friction heat and the volume of the plastic deformation metal are sufficient. Consequentially, there are no tunnel defects produced either at the AS or the RS in the skin. Generally, the horizontal flow and vertical flow occurs simultaneously in the stringer zone, and the flow resistance should be higher than that in the skin zone because the stringer is far away from the tool shoulder. When the welding axial force is relatively small or the heat input is insufficient, the downward force and tool rotation that result in the material transporting from the AS to the RS will not be so sufficient to push enough materials to refill the toe sites. Furthermore, because of the materials in the front of probe in the AS are more easily extruding and rotating to the zones of the RS, the material moves downward more obviously in the retreating side than that in the advancing side. Therefore, the refilling procedure is partially completed, and the toe corner of stringer nugget along advancing side is left empty with the continuous movement of tool probe along the joining line.

In order to study the influences of welding parameters on the tunnel defects in depth, some quantitative analysis is carried out. For the given tool geometry and forging axial force, only does the variation of the process parameters affect the tunnel defect areas. The relationship between tunnel defect area and tool rotating number per millimeter is shown in Fig. 8(a). It is easy to find that when the welding speed is kept constant the curve relationship could be simply described by the following equation:

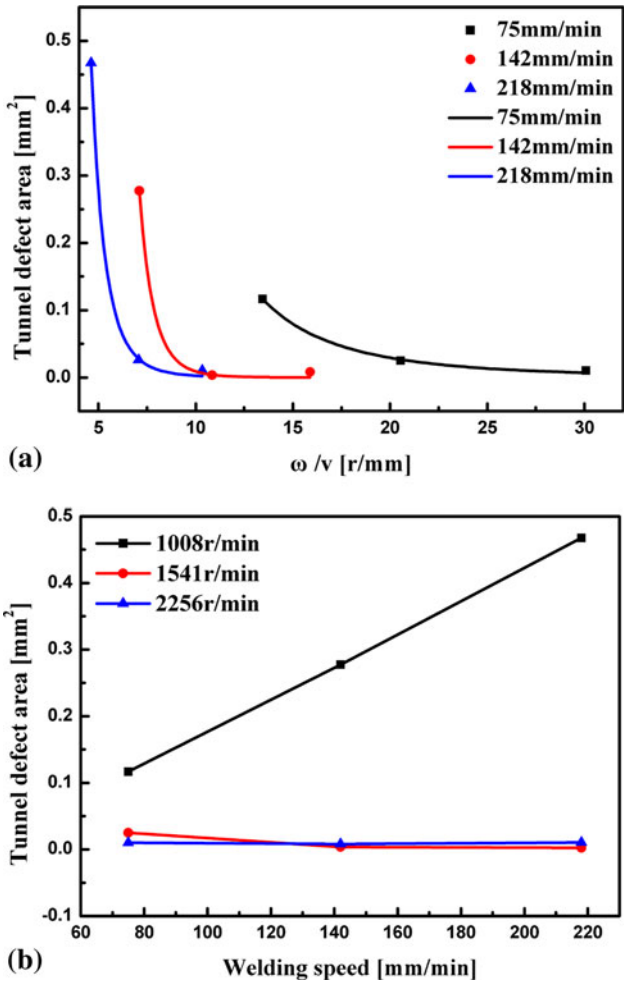

Fig. 8 The relationship between tunnel defects and process parameters (a) area of tunnel defects and rotation speed, (b) area of tunnel defects and welding speed

$$\mathrm{DA} = a\left(\frac{\omega}{v}\right)^{-b} \quad \text{(Eq 1)}$$

where DA is the tunnel defect area, v is the welding speed, ω is the tool rotation speed, a and b are the fitting coefficients, respectively. According to the equation, the tool characterized by larger rotation speed will generate more friction heat to decrease or eliminate the tunnel defects. Clearly, according to the variation trend, sound T-joints could be obtained when $11 < \omega/v < 16$ for a given welding speed of 142 mm/min.

Figure 8(b) shows the relationship between tunnel defects and welding speed for a given tool rotation speed. At the rotation speed of 1008 rpm, the tunnel defect areas are always larger and increase with the increase of the welding speed. But for 1541 and 2256 rpm, the defect areas are obviously smaller than that of 1008 rpm, because this phenomenon has a close relationship with heat input. The heat input of FSW can be indicated as following:

$$q = \frac{4}{3}\pi^2\mu\frac{P\omega}{v}R^3 \quad \text{(Eq 2)}$$

where, q is the heat input, μ is the friction coefficient, P is the axial pressure, v is the welding speed, ω is the tool rotation speed, and R is the shoulder radius. For the lower rotation speed,

the heat input q decreases with the increase of welding speed v. Consequently, the decreased volume of plastic material results in the insufficient material flow. But for the higher rotation speed, the heat input q is high enough to reduce the tunnel defect area.

3.3 Microhardness Profile

Figure 9 shows the microhardness variation along the different directions of the T-joint. Clearly, the welds are significantly softened around the welding center in the skin and under the NZ in the stringer. The lowest hardness, 75% of the BM, is 6 mm away from the welding center in the skin welds. In addition, the softened zone is narrower at the higher welding speed (218 mm/min) than that for the lower welding speeds (75 and 142 mm/min). Minimum values are related to the dissolution of precipitates during the thermal cycle of FSW. Previous studies showed that the BM contained a high density of fine needle-shaped precipitates which determined the hardness profiles of Al-Mg-Si alloys, but the fine needle-shaped precipitates were absent in the HAZ (Ref 22, 23). However, the recovery of microhardness is observed in the NZ due to fine grain, precipitation distribution of natural aging.

By referring to the aforementioned study on the microstructure, the amounts of precipitates in the TMAZ of stringer are similar to that in the HAZ of skin. So, the minimum value, up to 82% of the BM in the stringer, is 5.5 mm away from the top surface of the weld. What is more, it could be seen in Fig. 9(b) that the hardness of NZ in the top site corresponding to larger grains is lower than that in the middle site corresponding to smaller grains. In all the cases, the lowest hardness places might govern the fracture model of T-joints.

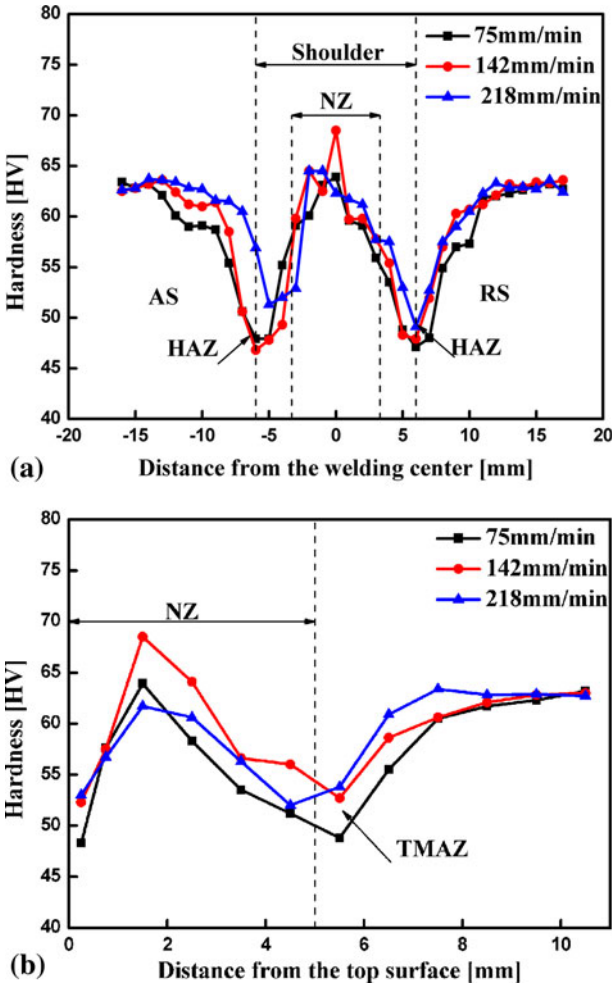

Fig. 9 Vickers microhardness profiles along T-joints at all welding conditions (a) hardness in the skin corresponding to 1541 rpm, (b) hardness in the stringer corresponding to 1541 rpm

3.4 Mechanical Properties

The significant microstructural evolution, the tunnel defects, and the non-uniformity of the hardness profiles, which appear in the welds, result in the change of the mechanical properties of T-joints. In order to estimate these changes, tensile tests are carried out in skin/transversal direction (T) and stringer/longitudinal direction (L), respectively. It should be pointed that the strength obtained from the testing is an average value including all the zones. The average ultimate tensile strength values versus welding speed are shown in Fig. 10.

It is noticeable that the tensile properties are higher in the stringer direction than those in the skin direction at the high rotation speeds. To a large extent, the tensile properties of T-joints are dependent on the welding defects and hardness distributions of joints (Ref 24). By referring to the above study, the hardness of TMAZ in the stringer is slightly higher compared to the hardness of HAZ in the skin. Meanwhile, the hardness near the top surface in the skin is severely softened. The combination of the two reasons leads to the tensile properties of stringers higher than those of skins.

Regardless of the rotation speed, the tensile strength in the skin direction has a little fluctuation in the range of welding speed 75-218 mm/min. But the strength increases a little with the increase of rotation speed. All the tensile strengths in the skin direction are in the range of 170-180 MPa, which are attributed to no defects in the skin welds and to fine grains in nuggets. Additionally, the rotation speeds have no effects on the tensile strength of T-joints at the welding speed of 218 mm/min. The T-joint in the skin direction performed the highest strength, 73.8% of BM, is under the condition of welding speed of 142 mm/min and rotation speed of 2256 rpm.

In the stringer direction, the tensile strength for lower rotation speed (1008 rpm) is obviously lower than those for

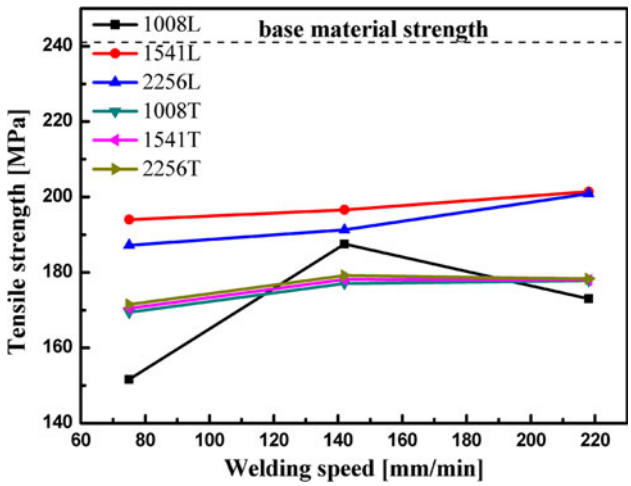

Fig. 10 The relationship between tensile strength and welding parameters

higher rotation speeds (1541 or 2256 rpm). The tensile strength increases with the increase of welding speed and rotation speed. The microstructures and defects of joining zones should be the key factors to influence the tensile properties. The size of grains is reduced by the increase of the welding speed for a given rotation speed, as shown in Table 2. Consequently, fine grains generate better mechanical properties. In all the cases, it is easy to get the information that the specimens welded at ω/v = 1541/218 r/mm exhibits the highest tensile strength that is equivalent to 83% of the BM. The reduction of tensile strength is in consistent with the decreased hardness value.

Because the different zones and welding defects have different resistances to deformation, the fractures mainly occur in the weakest sites of HAZ or the tunnel defects. All the fractures along the skin directions take place in the HAZ at the lowest hardness sites (Fig. 11a). When $\omega/v > 10$ r/mm the specimens fail in the HAZ of AS, and when $\omega/v < 10$ r/mm, the failed location is changed to the HAZ of RS. The fracture surfaces are parallel to the HAZ interface either in the AS or in the RS. The Vickers hardness information may give a perception of the failed location. Regardless of the welding condition, there are two lowest hardness zones corresponding to the HAZ on the two sides of weld center.

In the stringer direction, the fracture might occur in the TMAZ of stringer or the bonding interface (Fig. 11b, c). For the lower rotation speed of 1008 rpm, the fractures occur in the bonding interface of skin and stringer due to tunnel defects. The fracture surfaces of failure specimens are presented 90° plane perpendicular to the loading direction (Fig. 11b). In fact, the larger tunnel defects (the area is greater than 0.1 mm^2) in the AS apparently degrade the tensile properties of T-joints and cause the fracture at the bonding interfaces. While for the higher rotation speed of 1541 and 2256 rpm, most fractures occur in the stringer corresponding to the lowest hardness sites. In this situation, the macroscopic failures along the stringer direction are characterized by the limited necking and shearing deformations with the fracture surface inclined 45° to the tensile axis (Fig. 11c).

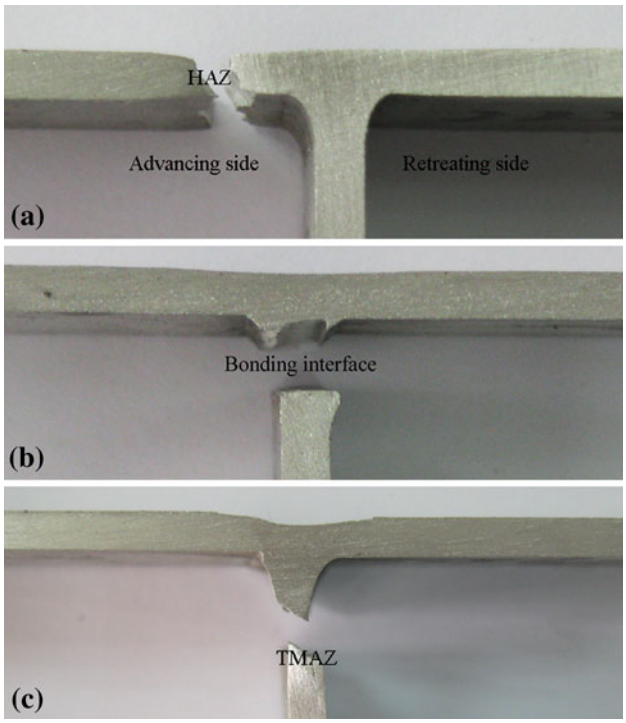

Fig. 11 Typical fracture location in testing in (a) skin direction failed in advancing side with welding parameter ω/v = 2256/142, (b) stringer direction failed at the bonding interface with welding parameter ω/v = 1008/142 r/mm, (c) stringer direction failed in the stringer with welding parameter ω/v = 2256/142 r/mm

It is found that the smaller tunnel defects (the area is less than 0.015 mm^2) and zigzag lines have no pronounced effects on the failed location in the stringer direction. It was also reported that the zigzag line had no effect on the tensile properties of as-welded butt-joints (Ref 18). However, the leftover oxide film of welds has been found to significantly affect the shear tensile strength of lap-joints (Ref 25). Moreover, it is noted that the strengths of welds for 1541 and 2256 rpm along the stringer direction are obviously higher than those for 1008 rpm in stringer direction. This is because the material flow of weld should reach the physical metallurgical joining at the higher rotation speed. Clearly, the fracture modes of T-welds are controlled by the lowest hardness sites and larger tunnel defect area in the stringer direction.

4. Conclusions

FSW of T-joints with 3 mm thickness for AA6061-T4 sheets has been successfully implemented. The microstructures, defects, hardness profiles, and tensile properties of T-joints have been discussed specifically. From this study, the main conclusions are summarized as follows:

The macrostructure and the microstructure are similar for all the welding conditions. From the whole view of the macrostructure of cross-section of the T-joint, the shape of NZ is an inverted trapezoid with curved edge, and there are zigzag lines across the weld. The microstructure features in the skin welds have the same patterns as those of butt-joints. The unique microstructures of T-joints are the two fillet zones which are made of fine grains.

The tunnel defects tend to occur at the toe corner of stringer nugget along advancing side. When the welding speeds are kept constant, the tunnel defect area has a negative exponent relationship with the rotation speed.

Two lower microhardness zones are around the welding center in the skin welds, and the minimum value of hardness is 75% of the BM regardless of process parameters. The stringer TMAZ is also softened and its minimum hardness is reduced over 17% compared to the BM.

The tensile strengths are higher in the stringer direction than those in the skin direction at the same welding conditions. All the fracture sites in the skin direction take place in the HAZ corresponding to the lowest hardness sites. And the tensile strengths are ranged from 170 to 180 MPa for all specimens. In the stringer direction, the larger tunnel defects (the area was greater than 0.1 mm^2) in the AS would reduce the tensile properties of T-joints and cause the joints to fracture at the bonding interface. The smaller tunnel defects (the area was less than 0.015 mm^2) and zigzag lines have no pronounced effects on the failed locations. In this testing, the specimen welded at ω/v = 1541/218 r/mm along the stringer direction exhibits the highest tensile strength which is equal to 83% of BM.

Acknowledgments

This work is supported by the National Nature Science Foundation of China (No. 50775159)

References

1. R.S. Mishra and Z.Y. Ma, Friction Stir Welding and Processing, *Mater. Sci. Eng. Rep.*, 2005, **50**(1–2), p 1–78
2. S.M.O. Tavares, P.C.M. Azevedo, B. Emilio, V. Richter-Trummer, M.A.V. Figueiredo, P. Vilaca, and P.M.S.T. de Castro, Friction Stir Welding of T-Joints in Dissimilar Aluminum Alloys, *Imece2008: Proceedings of the ASME International Mechanical Engineering Congress and Exposition, ASEM*, 2008 (Boston), American Society of Mechanical Engineers, 2009, p 265–273
3. V. Richter-Trummer, S.M.O. Tavares, P.M.G.P. Moreira, and P.M.S.T. de Castro, Friction Stir Welding of Aluminum Alloys and Damage Tolerance of Integral Monolithic Structures, *Mechanika*, 2008, **5**, p 18–22
4. M.L. Penalva, A. Otaegi, J. Pujana, and A. Rivero, Development of a New Joint Geometry for FSW, *AIP Conference Proceedings*, Vol 1181, V.J. Segui and M.J. Reig, Ed., American Institute of Physics, Alcoy, Spain, 2009, p 1–11
5. G. Buffa, L. Fratini, F. Micari, and R. Shivpuri, Material Flow in FSW of T-joints: Experimental and Numerical Analysis, *Int. J. Mater. Form.*, 2008, **1**(Suppl 1), p 1283–1286
6. R. Sandstrom, M. Ericsson, and L.Z. Jin, Fatigue Properties of Friction Stir Overlap Welds, *Int. J. Fatigue*, 2007, **29**(1), p 57–68
7. L. Fratini, G. Buffa, F. Micari, and R. Shivpuri, On the Material Flow in FSW of T-joints: Influence of Geometrical and Technological Parameters, *Int. J. Adv. Manuf. Technol.*, 2009, **44**(5–6), p 570–578
8. L. Fratini, F. Acerra, G. Buffa, and G. Troiano, On the FSW of AA2024-T4 and AA7075-T6 T-joints: An Industrial Case Study, *Int. J. Adv. Manuf. Technol.*, 2010, **48**(9–12), p 1149–1157
9. L. Fratini, G. Buffa, and R. Shivpuri, Influence of Material Characteristics on Plastomechanics of the FSW Process for T-joints, *Mater. Des.*, 2009, **30**(7), p 2435–2445
10. P.A. Fleming, C.E. Hendricks, D.M. Wilkes, G.E. Cook, and A.M. Strauss, Automatic Seam-Tracking of Friction Stir Welded T-joints, *Int. J. Adv. Manuf. Technol.*, 2009, **45**(5–6), p 490–495
11. K. Erbsloh, C.D. Donne, and D. Lohwasser, Friction Stir Welding of T-joints, *Materials Science Forum*, Vol 426–432, T. Chandra, J.M. Torralba, and T. Sakai, Ed., Trans Tech Publications, Leganes, Madrid, Spain, 2003, p 2965–2970
12. S.M.O. Tavares, R.A.S. Castro, V. Richter-Trummer, P. Vilaca, P.M.G.P. Moreira, and P.M.S.T. de Castro, Friction Stir Welding of T-joints with Dissimilar Aluminum Alloys: Mechanical Joint Characterization, *Sci. Technol. Weld. Join.*, 2010, **15**(4), p 312–318
13. L. Fratini, G. Buffa, L. Filice, and F. Gagliardi, Friction Stir Welding of AA6082-T6 T-joints: Process Engineering and Performance Measurement, *Proc. Inst. Mech. Eng. B-J. Eng.*, 2006, **220**(5), p 669–676
14. L. Donati, L. Tomesani, and A. Morri, Structural T-joint Produced by Means of Friction Stir Welding (FSW) with Filling Material, *Int. J. Mater. Form.*, 2009, **2**(Suppl1), p 295–298
15. G. Buffa, G. Campanile, L. Fratini, and A. Prisco, Friction Stir Welding of Lap Joints: Influence of Process Parameters on the Metallurgical and Mechanical Properties, *Mater. Sci. Eng. A*, 2009, **519**(1–2), p 19–26
16. R.S. Mishra, M.K. Yadava, Y.L. Chen, B. Carlson, and G.J. Grant, Study of Friction Stir Joining of Thin Aluminum Sheets in Lap Joint Configuration, *Sci. Technol. Weld. Join.*, 2010, **15**(1), p 70–75
17. S.S. Di, X.Q. Yang, D.P. Fang, and G.H. Luan, The Influence of Zigzag-Curve Defect on the Fatigue Properties of Friction Stir Welds in 7075-T6 Al Alloy, *Mater. Chem. Phys.*, 2007, **104**(2–3), p 244–248
18. H.J. Liu, Y.C. Chen, and J.C. Feng, Effect of Zigzag Line on the Mechanical Properties of Friction Stir Welded Joints of an Al-Cu Alloy, *Scripta Mater.*, 2006, **55**(3), p 231–234
19. K. Elangovan and V. Balasubramanian, Influences of Tool Probe Profile and Tool Shoulder Diameter on the Formation of Friction Stir Processing Zone in AA6061 Aluminum Alloy, *Mater. Des.*, 2008, **29**(2), p 362–373
20. Z.W. Chen, T. Pasang, and Y. Qi, Shear Flow and Formation of Nugget Zone During Friction Stir Welding of Aluminum Alloy 5083-O, *Mater. Sci. Eng. A*, 2008, **474**(1–2), p 312–316
21. H. Zhang, H.Q. Wu, J.H. Huang, S.B. Lin, and L. Wu, Effect of Welding Speed on the Material Flow Patterns in Friction Stir Welding of AZ31 Magnesium Alloy, *Rare Metals*, 2007, **26**(2), p 158–162
22. P.M.G.P. Moreira, T. Santos, S.M.O. Tavares, V. Richter-Trummer, P. Vilaca, and P.M.S.T. de Castro, Mechanical and Metallurgical Characterization of Friction Stir Welding Joints of AA6061-T6 with AA6082-T6, *Mater. Des.*, 2009, **30**(1), p 180–187
23. Y.S. Sato, M. Urata, and H. Kokawa, Parameters Controlling Microstructure and Hardness During Friction-Stir Welding of Precipitation-Hardenable Aluminum Alloy 6063, *Metall. Mater. Trans. A*, 2002, **33**(3), p 625–635
24. H.J. Liu, H. Fujii, M. Maeda, and K. Nogi, Tensile Properties and Fracture Locations of Friction-Stir-Welded Joints of 2017-T351 Aluminum Alloy, *J. Mater. Process. Technol.*, 2003, **142**(3), p 692–696
25. A. Elrefaey, M. Gouda, M. Takahashi, and K. Ikeuchi, Characterization of Aluminum/Steel Lap Joint by Friction Stir Welding, *J. Mater. Eng. Perform.*, 2005, **14**(1), p 10–17